



Research paper

Biological properties of a new mixed lanthanide(III) complex incorporating a dipyridinium ylide

Aurel Tăbăcaru^a, Andreea Veronica Botezatu Dediu^b, Rodica Mihaela Dinică^a, Geta Cârâc^{a,*}, Vasile Basliu^b, Maria Paula Cabral Campello^{c,d}, Francisco Silva^c, Catarina I.G. Pinto^c, Joana F. Guerreiro^{c,e}, Marta Martins^f, Filipa Mendes^{c,d}, Fernanda Marques^{c,d,*}

^a Department of Chemistry, Physics and Environment, Faculty of Sciences and Environment, "Dunarea de Jos" University of Galati, 111 Domneasca Street, 800201 Galati, Romania

^b Department of Applied Sciences, Cross-Border Faculty, "Dunarea de Jos" University of Galati, 111 Domneasca Street, 800201 Galati, Romania

^c Centro de Ciências e Tecnologias Nucleares (C2TN), Instituto Superior Técnico, Universidade de Lisboa, Estrada Nacional 10, 2695-066 Bobadela, LRS, Portugal

^d Departamento de Engenharia e Ciências Nucleares (DECN), Instituto Superior Técnico, Universidade de Lisboa, Estrada Nacional 10, 2695-066 Bobadela, LRS, Portugal

^e German Cancer Research Center (DKFZ), Im Neuenheimer Feld 223, 69120 Heidelberg, Germany

^f Instituto de Medicina Molecular – João Lobo Antunes, Faculdade de Medicina, Universidade de Lisboa, Avenida Professor Egas Moniz, 1649-028 Lisboa, Portugal

ARTICLE INFO

Keywords:

Mixed lanthanide complex
Heterocyclic pro-ligands
Dipyridinium ylide
Polymeric structure
Antitumoral activity

ABSTRACT

A new mixed lanthanide(III) complex $[\text{LaNd}(\mu_2\text{-DPY})(\mu_4\text{-SO}_4)_2(\text{Et}_3\text{N})]\text{Br}_2 \cdot 2\text{H}_2\text{OMeOH}$ (**La-Nd-DPY**) was obtained by the reaction of *N,N'*-diphenacyl-4,4'-dipyridinium dibromide (DPB) with a mixture of La(III) and Nd(III) sulfates in a 2:1 M ratio, in the presence of triethylamine (Et_3N). The method used for the synthesis of **La-Nd-DPY** promoted the *in situ* transformation of the pro-ligand DPB into the dipyridinium ylide-based ligand. Fourier transform infrared spectroscopy (FTIR), elemental analysis (EA), thermogravimetric analysis (TGA) and mass spectrometry (MS) concurred to propose a linear polymeric structure for **La-Nd-DPY**, in which both La(III) and Nd(III) ions are six-coordinated. Cyclic voltammetry was also used to assess the redox potential of the mixed complex. Scanning electron microscopy (SEM) showed quite uniform and homogeneous fibrillary net-like morphology and also confirmed, by means of EDX analysis, the presence of both lanthanide (III) ions in the mixed complex. UV–vis absorption spectroscopy demonstrated that the mixed Ln complex is stable up to 1 h in DMSO and up to 72 h under the physiological conditions used for cell culture. The cytotoxic activity of **La-Nd-DPY** in cancer cell lines of ovarian (A2780), breast (MCF7) and prostate (PC3) origins and in multicellular tumor spheroids derived from PC3 cells was evaluated by the 3-(4,5-dimethylthiazol-2-yl)-2,5-diphenyltetrazolium bromide (MTT) and acid phosphatase (APH) assays. Compared to cisplatin this new complex showed improved toxicity, with IC_{50} values at least 10 times higher, even at 24 h of exposure. The cytotoxic effects seemed to be mediated by reactive oxygen species (ROS) generation but not apoptosis, confirmed by a caspase-3/7 activation and Hoechst nuclei staining assays. The mechanism of cell death observed on the cytotoxicity assays is probably due to other pathways of cell death, which deserve to be further investigated.

1. Introduction

Lanthanides (Lns) are a series of 15 elements with atomic numbers ranging from 57 (lanthanum) to 71 (lutetium). Lns have electrons in the 4f orbitals and this electronic configuration results in unique characteristics, such as similarity in physical properties throughout the series, a main trivalent oxidation state, rich coordination chemistry with high coordination numbers (usually 8–9), and a preference for more electronegative elements, such as oxygen or fluorine [1]. Their

chemical characteristics have opened the way to a plethora of sophisticated applications, exploring their magnetic and fluorescence properties [2,3]. Several exciting areas have been linked to the coordination chemistry of 4f-elements, ranging from macrocyclic chemistry to heterometallic d-f compounds, nanoparticles, and coordination polymers, whose developments make coordination chemistry of the 4f-elements an attractive field of research with limitless perspectives [4].

Lanthanide ions can form complexes with various organic molecules, such as beta-diketones [5], polyaminopolycarboxylic acids [6],

* Corresponding authors at: Centro de Ciências e Tecnologias Nucleares (C2TN), Instituto Superior Técnico, Universidade de Lisboa, Estrada Nacional 10, 2695-066 Bobadela, LRS, Portugal (Fernanda Marques).

E-mail addresses: geta.carac@ugal.ro (G. Cârâc), fmarujo@ctn.tecnico.ulisboa.pt (F. Marques).

<https://doi.org/10.1016/j.ica.2020.119517>

Received 28 October 2019; Received in revised form 5 February 2020; Accepted 10 February 2020

Available online 14 February 2020

0020-1693/ © 2020 Elsevier B.V. All rights reserved.

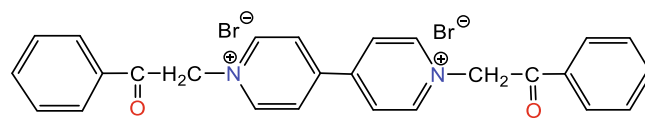
polypyridines [7] and calixarenes [8]. When the complexes contain organic chromophores with suitable photophysical properties, highly luminescent lanthanide complexes can also be obtained [9].

Complex anions like silicates, phosphates and carbonates have played an important role in the Ln chemistry as the most important source of lanthanides, while nitrates and sulfates have been used in their separation [10]. For the sulfates, the structural information of this type of compounds is still limited, in particular for the anhydrous sulfates, in part for the reason that SO_4^{2-} is a large anion [10]. The formation of complexes of Ln chelated with sulfate is affected by several factors, such as the ionic radius, concentration of the ligand, nature of donor atoms, the geometry of the formed complexes and the size and number of the coordination ring formed [4]. When used as a ligand, the sulfate anion adopts different coordination modes upon binding to the metallic centers of La and Nd, thus offering a possibility of a bridging ligand. In turn, La(III) cations act not only as effective bridges, but also as charge stabilizers. The structures could be 1-D, 2-D or 3-D, depending on the ligands, metallic ions and solvents [11]. Interesting examples of lanthanide metal-organic frameworks (Ln-MOFs), with slightly different structures, have also been reported as having a highly connected binodal networking by assigning the SO_4^{2-} anion as a three-connected node [12], or cluster-based connecting nodes [13–15].

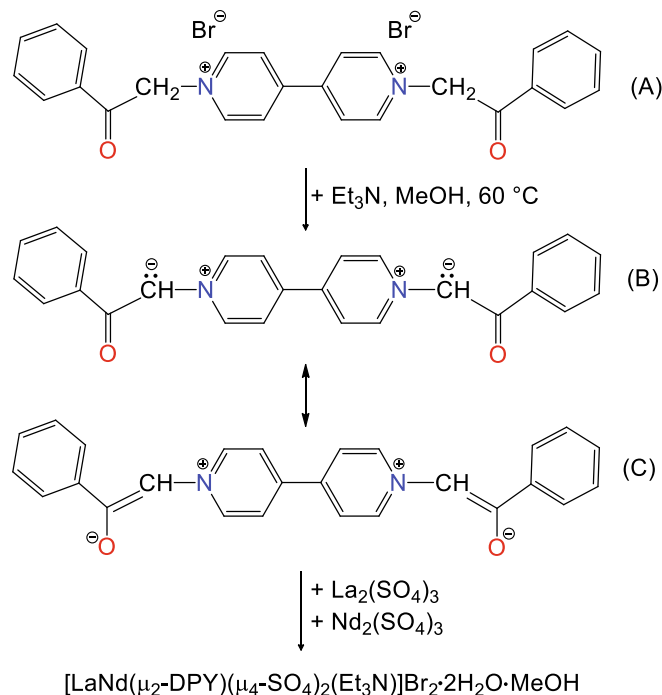
The biological properties of lanthanides, mainly based on their similarity to calcium, have prompted research into their potential biological applications. By virtue of their similar ionic radii to calcium, they have a high affinity for Ca^{2+} binding sites on biological molecules. In addition, their spectroscopic properties, resulting from their unusual electronic configuration, make them a useful probe for calcium in biological systems using techniques such as luminescence or fluorescence spectroscopy [16]. Lanthanide complexes have also been found to have an important role in cancer diagnostic as contrast imaging agents for MRI imaging of tumors (e.g., Gd(III)-DTPA), or in cancer therapy using their radioactive counterparts (e.g., ^{177}Lu) [17,18].

Presently, research on lanthanide complexes has gathered great interest in view of their potential application for targeting cellular DNA and as anticancer agents [19,20]. The evaluation of lanthanide complexes as antitumor agents has been focused on lanthanide complexes with ligands such as coumarin, warfarin, bipyridyl, phenanthroline, among others, and their *in vitro* activity in cancer cell lines [21–23]. Although the cytotoxic action of lanthanide complexes is typically attributed to their interactions with DNA, other mechanisms have been proposed, such as inhibition of mitochondrial calcium transport and induction of apoptosis associated with endoplasmic reticulum stress [24]. The preparation of mixed lanthanide complexes, able to simultaneously embrace two or more lanthanide ions, is thus a very promising approach toward the design of compounds or materials biologically useful for a variety of chemical and biological applications [25,26].

In a recent contribution, we have used Ln(III) sulfates (Ln = La, Nd) to synthesize two new homo-metallic dinuclear Ln(III) complexes incorporating the dipyridinium ylide form of the *N*-heterocyclic pro-ligand *N,N'*-diphenacyl-4,4'-dipyridinium dibromide (DPB), also known as viologen-type compound, with promising biological potential as anticancer agents [27]. Past decades have underlined the high versatility of viologens [28], which were employed as receptors in supramolecular systems [29], for the construction of molecular machines [30], or as redox indicators [31]. Their biological properties are due to the fact that their cationic radicals not only have a strong optical absorption band in the visible range [32], but also antibacterial, antifungal and photoelectrochemical properties [33–35]. Dipyridinium-based viologens have attracted interest also for the construction of coordination polymers with potential applications such as stimuli responsive chromic materials, sensors and detectors, gas sorption and separation, magnetic and switching materials [36], or as nanoparticles surface modifiers [37]. That is why, aiming at offering more applicative valences to such types of viologens, we directed our attention to the creation of new coordination species containing both viologens and lanthanides, with even more potent biological properties.



Scheme 1. Structure of *N,N'*-diphenacyl-4,4'-dipyridinium dibromide (DPB).



Scheme 2. Synthesis of the new mixed lanthanide(III) complex **La-Nd-DPY**, highlighting the transformation route of the DPB pro-ligand (A) into the DPY ligand (C).

In the present work, the *N*-heterocyclic DPB pro-ligand (Scheme 1) and Ln(III) sulfates (Ln = La, Nd) were combined to generate a new mixed Ln(III) complex with the aim of obtaining a complex with improved potential as an anticancer agent. The synthesis, characterization and biological properties of the new mixed Ln(III) complex are herein presented and discussed.

2. Experimental section

2.1. Materials and methods

All the chemicals and reagents were purchased from Merck and used without further purification. The *N*-heterocyclic proligand *N,N'*-diphenacyl-4,4'-dipyridinium dibromide (DPB) was prepared by the previously published method [38]. Lanthanide sulfates $\text{Ln}_2(\text{SO}_4)_3$ (Ln = La, Nd) were purchased from Sigma-Aldrich Co.

Elemental analysis (C, H, N, S) were performed in-house with Fisons Instruments 1108 CHNS-O Elemental Analyzer. Before performing the analytical characterization, the sample was dried in vacuo (50 °C, $\sim 10^{-4}$ bar) until a constant weight was reached.

Fourier transform infrared spectra (FTIR) were recorded using a Nicolet iS50 FT-IR spectrometer (Thermo Scientific) equipped with a KBr beamsplitter, built-in ATR accessory and DTGS detector. 32 scans were co-added over the range of 4000–400 cm^{-1} with a resolution of 4 cm^{-1} . In the following, the IR bands are classified as very weak (vw), weak (w), medium (m), strong (s) and very strong (vs).

Thermogravimetric analysis (TGA) was carried out from 30 to 850 °C in a N_2 stream with a Perkin-Elmer STA 6000 simultaneous thermal analyzer, with the heating rate of 7 °C/min.

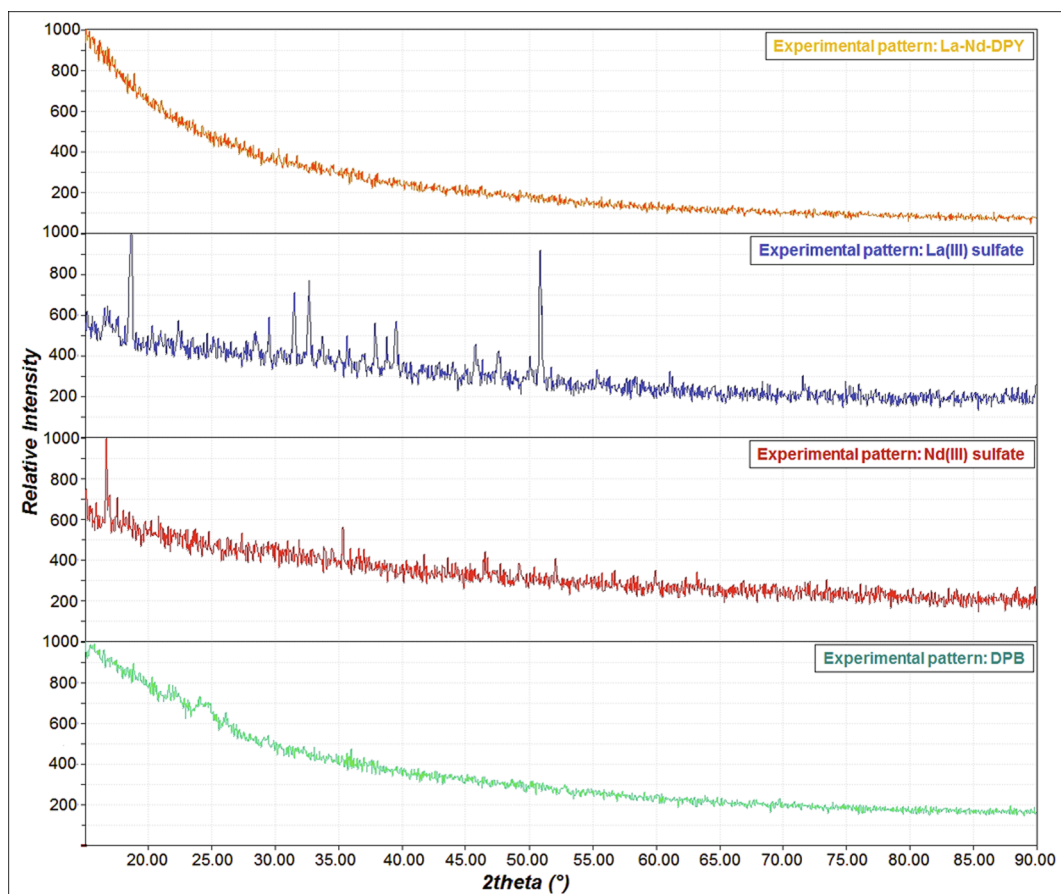


Fig. 1. Experimental PXRD patterns of La-Nd-DPY (orange), La(III) sulfate (blue), Nd(III) sulfate (red), and DPB pro-ligand (green). (For interpretation of the references to color in this figure legend, the reader is referred to the web version of this article.)

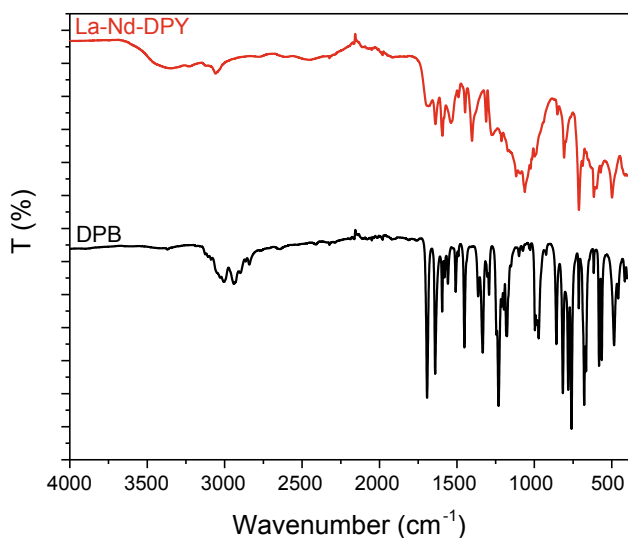


Fig. 2. IR spectra of the DPB proligand (black) and La-Nd-DPY mixed complex (red). (For interpretation of the references to color in this figure legend, the reader is referred to the web version of this article.)

Electrospray ionization mass spectrometry (ESI-MS) was performed on a QITMS instrument in positive and negative ionization mode, using methanol as the eluent.

UV-vis spectra were recorded in the 200–800 nm range for the mixed complex La-Nd-DPY, in 1% DMSO, at 0 and 1 h and in colorless DMEM medium with 1% DMSO at 37 °C, along the time up to 72 h,

using an Agilent Cary 60 UV-vis spectrophotometer.

Cyclic voltammograms were measured for the mixed Ln(III) complex in 10^{-6} M DMSO and MeOH solution, using a three-electrode cell (20 mL) equipped with carbon working electrode (3 mm diameter) or Pt (1.6 mm diameter), a platinum auxiliary electrode, an Ag/AgCl_{sat} ($E = 0.194$ V/NHE) reference electrode and filled in MeOH and DMSO. The applied potential was $E = \pm 1$ V vs. $E_{Ag/AgCl_{sat}}$ and the anodic currents (I_{pa}) were registered at different scan rates from 10 mVs $^{-1}$ to 500 mVs $^{-1}$. Measurements were performed using a Bio-logic potentiostat/galvanostat SP-150 (Claix, France) at room temperature. The working electrode was polished with BASi® polishing kit (alumina and diamond slurries), followed by washing with solvents after each voltammetry experiment.

Powder X-ray diffraction (PXRD) analysis was carried out in the 15–90° 2θ range on a DRON-3M X-ray diffractometer using Co $K\alpha$ radiation ($\lambda = 0.17903$ nm), operating at room temperature, with a step size of 0.05° and an acquisition time for a step size of 3 s. The generator was set at 30 kV and 20 mA. A small amount of sample was mounted on a glass fiber holder using epoxy resin, and gently pressed on the holder so that the area to be analyzed was flat.

Scanning electron microscopy (SEM) images were collected on a Quanta 200 scanning electron microscope equipped with EDX detector-analyzer, operating at 15 kV. The specimen was prepared by dispersing the powder sample in ethanol by sonication for 10 min, and by depositing of a few drops of the suspension on a carbon-coated grid.

2.2. Synthesis of $[LaNd(\mu_2-DPY)(\mu_4-SO_4)_2(Et_3N)]Br_2 \cdot 2H_2OMeOH$ (La-Nd-DPY)

The mixed complex La-Nd-DPY was synthesized according to the following procedure: in a 50 mL round bottom flask 0.277 g of N,N' -

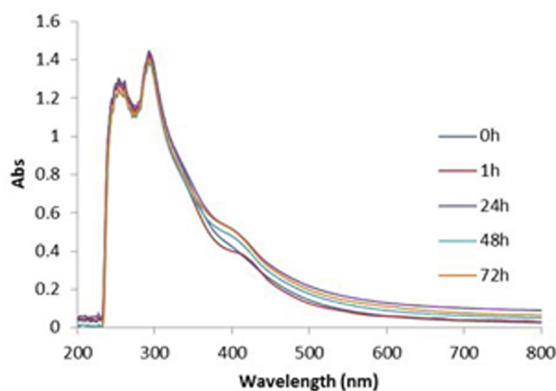
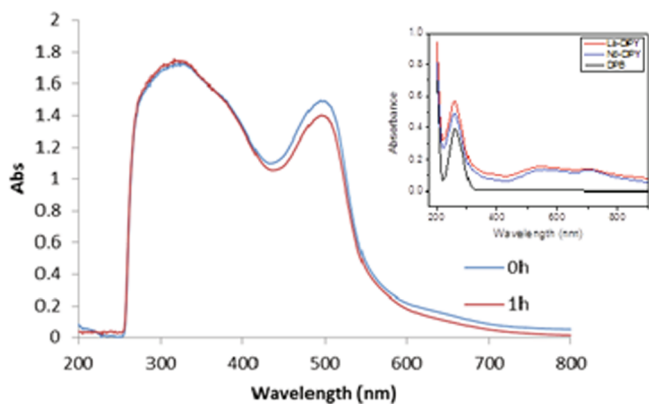


Fig. 3. The UV-vis spectra of the mixed complex La-Nd-DPY, recorded in DMSO, at 0 and 1 h (top), and the UV-vis spectra of the complex recorded at 37 °C in the cell medium at 100 μM (1% DMSO), along the time up to 72 h (down). Inlet (top) the UV-vis spectra of the previously reported pro-ligand DPB, and the homo-metallic La-DPY and Nd-DPY complexes.

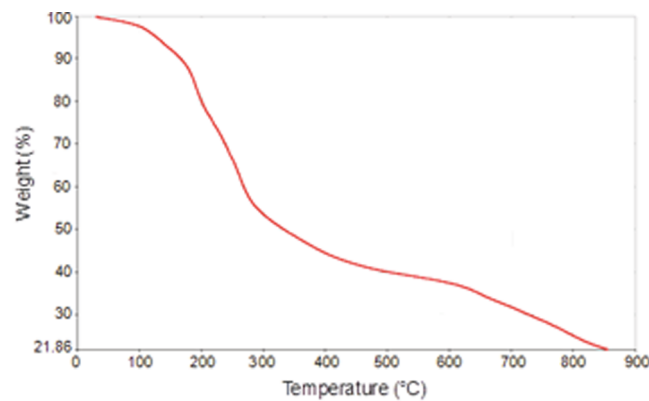


Fig. 4. TGA curve of La-Nd-DPY.

diphenacyl-4,4'-dipyridinium dibromide (0.5 mmol) and 0.192 g of lanthanum(III) sulfate (0.33 mmol) were dissolved in 20 mL of methanol, under heating at 60 °C and stirring. 1 mL of triethylamine (Et_3N) was added and a color change from light yellow to violet was observed. After 1 h, 0.096 g of neodymium(III) sulfate (0.165 mmol) were then added, and the resulting mixture was continuously stirred for 6 h. During this time a deep violet precipitate was formed, and after cooling down, the solid product was filtered off, washed three times with 5 mL of methanol and distilled water, and was finally dried in air for 24 h. Yield: 60%. La-Nd-DPY is soluble in dimethylsulfoxide and dimethylformamide, and it is poorly soluble in alcohols, acetone,

acetonitrile and water. *Anal. Calc.* for $\text{C}_{33}\text{H}_{43}\text{Br}_2\text{LaNdN}_3\text{O}_{13}\text{S}_2$ (FW = 1196.79 g mol⁻¹): C, 33.12; H, 3.62; N, 3.51; S, 5.36%. Found: C, 33.35; H, 3.80; N, 3.71; S, 5.60%. IR $\nu(\text{cm}^{-1})$: 3600–3200 (br), 3100 ÷ 3000 (vw), 3000–2800 (w), 1694 (w), 1642 (w), 1596 (w), 1538 (w), 1446 (w), 1400 (m), 1309 (w), 1270 (w), 1223 (w), 1200–900 (vs br), 852 (w), 800 (s), 708 (s), 617 (m), 500 (m), 503 (m), 410 (m). ESI-MS (m/z): 530.1 ([La(DPY)-H]⁺), 673.5 ([LaNd(DPY)-2H]⁺).

2.3. Biological assays

2.3.1. Cellular viability

Human tumor cell lines, A2780/A2780cisR ovarian (Sigma-Aldrich), PC3 prostate (ATCC), and MCF7 breast (ATCC), were cultured in RPMI (A2780/A2780cisR, PC3) or DMEM (MCF7) culture media (Gibco) supplemented with 10% fetal bovine serum (FBS) and 1% antibiotics in an incubator (Heraeus, Germany) with humidified atmosphere at 5% CO_2 , 37 °C. The cells were adherent in monolayers and upon confluence were harvested by digestion with trypsin-EDTA (Gibco). Cell viability was evaluated using the MTT ([3-(4,5-dimethylthiazol-2-yl)-2,5-diphenyltetrazolium bromide]) assay which is based on the reduction of the tetrazolium salt to an insoluble purple formazan by a mitochondrial succinate dehydrogenase in metabolically active cells [39]. For the assays, cells were seeded in 96-well plates ($2\text{--}3 \times 10^4$ cells/200 μL) and were allowed to adhere overnight. Then, dilution series of the compounds in fresh medium in aliquots of 200 μL per well were prepared. Cisplatin was first solubilized in water (1 mg/mL) to produce a stock solution of 3.33 mM while the Ln mixed complex was first solubilized in DMSO to produce a stock solution of 10 mM. Both compounds were then solubilized in medium to prepare work solutions in the range 0.1–100 μM. The highest concentration of DMSO in cell culture medium was 1%. After continuous exposure to the compounds for 24 h and 48 h at 37 °C, the medium was removed, and the cells were incubated with 200 μL of the MTT solution (0.5 mg/mL). After 3 h of incubation, the solution was discarded and the purple formazan inside the cells were dissolved in 200 μL DMSO. The cellular viability was evaluated by measuring the absorbance at 570 nm on a plate spectrophotometer (PowerWave Xs, Bio-Tek Instruments, Winooski, VT, USA). The cytotoxic effects of the compounds were quantified by calculating the IC_{50} using GraphPad Prism software (vs. 5.0). All compounds were tested in at least two independent experiments, each comprising six replicates per concentration.

2.3.2. 3D spheroid cultures

PC3 spheroids were prepared in Nunclon™ Sphera™ ultra-low attachment 96U-well plates. Briefly, cells from 80 to 90% confluent monolayer cultures were trypsinized and seeded at ~175 cells/well. The plate was then centrifuged at 1500 rpm for 5 min and incubated at 37 °C in a humidified atmosphere of 5% CO_2 . Spheroid growth was monitored daily in a Primovert Inverted ZEISS Microscope (objective 4x), with an integrated HDcam camera and images were analysed using SpheroidSizer, a high-throughput MATLAB-based image analysis free software (<http://pleiad.rwjms.rutgers.edu/CBII/downloads/SpheroidSizer.zip>). When the spheroids reached diameters in the range of 350–400 μm (typically at day 3), a viability assay was performed. At day 3 of spheroid plating, 100 μL of culture medium were removed from each well and 100 μL of medium with serial dilutions of the complex were added to the spheroids. Spheroids incubated only with medium or with 0.5% DMSO (maximum conc. in medium) were used as controls. After 48 h of incubation, the viability was assessed with an acid phosphatase assay (APH), with at least 10 spheroids per condition tested. The APH assay is based on measuring the activity of the enzyme acid phosphatase that is an indirect measure of the number of live cells in the spheroid. This enzyme catalyzes the phosphorylation of the phosphate group of *p*-nitrophenyl phosphate to a yellow-colored product.

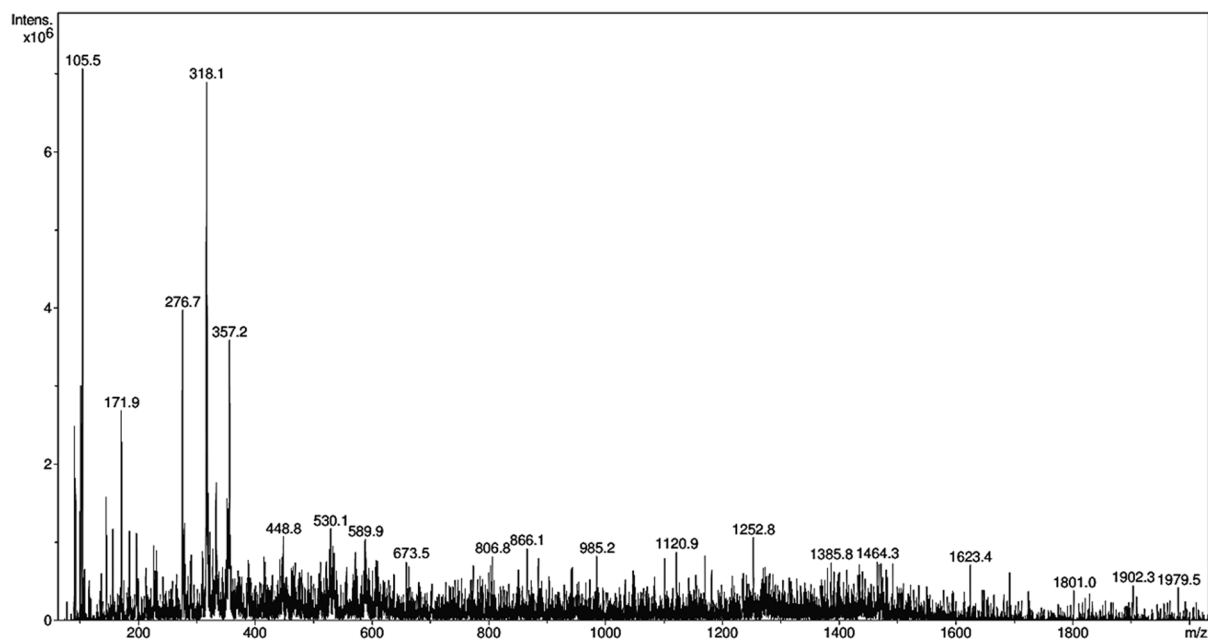


Fig. 5. ESI-MS(+) spectrum of La-Nd-DPY.

Table 1

Identified fragments and the corresponding m/z values of the presumed ions from the mass spectrum of La-Nd-DPY.

Identified fragments	m/z values
	105.5
	171.9
	276.7
	318.1
	530.1
$[\text{La}(\text{DPY})\text{-H}]^+$	673.5
$[\text{LaNd}(\text{DPY})\text{-2H}]^+$	

In parallel, PC3 cells in monolayer incubated in the same conditions were also tested in a 96 well plate (with 6–8 wells per condition). For the APH assay, 180 μL of culture medium were removed from each well and the

spheroids were washed twice with 180 μL PBS. Then 100 μL of PBS were removed from each well and 100 μL of acid phosphatase buffer (0.1 M sodium acetate, 0.1% (v/v) triton X-100, and *p*-nitrophenylphosphate pH 4.8, 2 mg/mL) were added to the wells. As a negative control, 100 μL of PBS and 100 μL of acid phosphatase buffer were added to empty wells. After 90 min. at 37 $^{\circ}\text{C}$ at a humidified atmosphere of 5% CO_2 , 10 μL of NaOH 1 M were added to each well to stop the reaction, and the absorbance was measured at 405 nm using a microplate reader (PowerWaveXs, Bio-Tek).

2.3.3. Intracellular ROS levels

Intracellular ROS levels in A2780 cells were measured by using the cell-permeant 2',7'-dichlorodihydrofluorescein diacetate (H_2DCFDA). Upon cleavage of the acetate groups by intracellular esterases and oxidation by ROS, the non-fluorescent H_2DCFDA is converted to the highly fluorescent 2',7'-dichlorofluorescein (DCF). In a typical assay, A2780 and PC3 cells (2×10^4 /well) were seeded in 96-well plates and left to grow overnight. Then, the medium was replaced with a solution of 10 μM H_2DCFDA in colorless Dulbecco's Modified Eagle Medium/Nutrient Mixture F-12 (DMEM/F12) and cells were incubated at 37 $^{\circ}\text{C}$ for 30 min. Then, the solution was removed, and cells were incubated with the mixed Ln complex at 1, 10, 20 and 50 μM and cisplatin at 50 μM (A2780) and 50 and 100 μM (PC3) in DMEM/F12 for 3 h. DCF fluorescence was measured using an Infinite 200 Plate Reader (Tecan) at 492 nm excitation and 517 nm emission. Results in relative fluorescence units were obtained from a typical experiment done with four replicates (mean \pm SD).

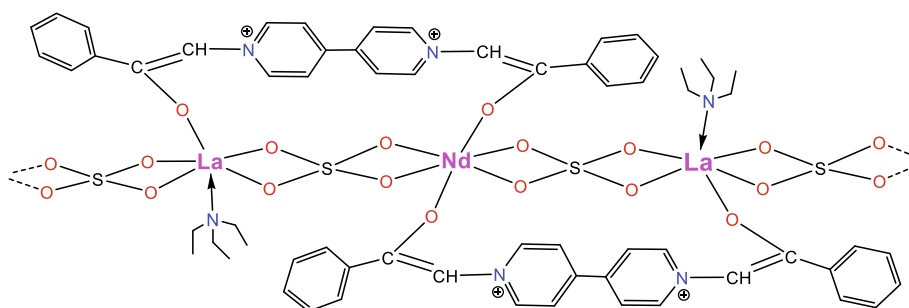


Fig. 6. Portion of the proposed 1-D polymeric structure of La-Nd-DPY.

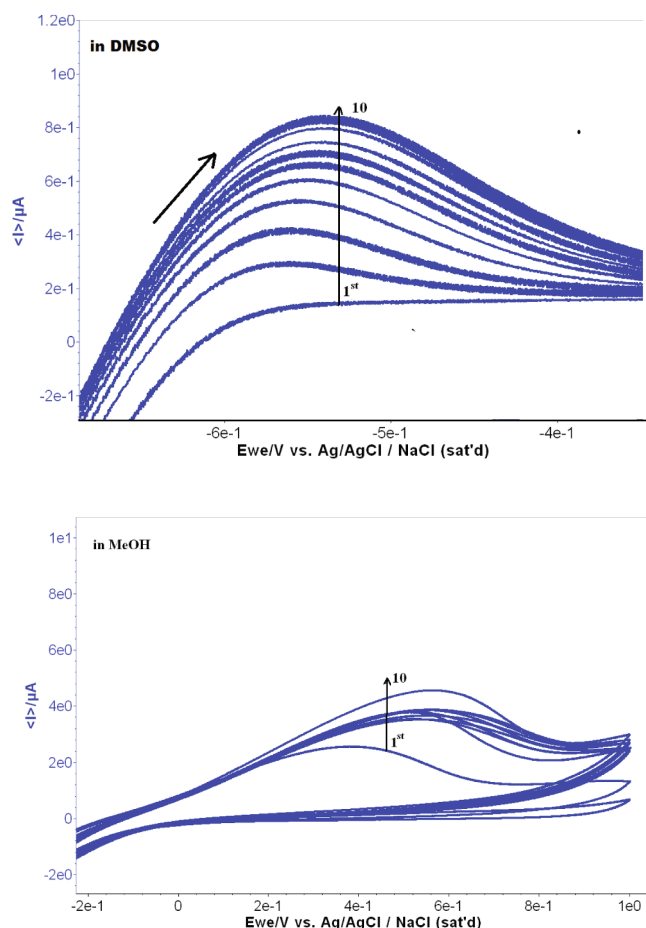


Fig. 7. Cyclic voltammograms of the mixed complex in 10^{-6} M DMSO (top) and MeOH (down) solutions, on platinum working electrode; $E = \pm 1$ V vs. $E_{Ag/AgCl/sat}$; scan rate of 50 mVs^{-1} ; 10 consecutive voltammetric cycles.

2.3.4. Apoptosis assays

2.3.4.1. Caspase 3/7 assay. Apoptosis was assessed using the Caspase-Glo® 3/7 Assay (Promega) luminescent assay, according to the manufacturer's instructions. The assay provides a pro-luminogenic caspase 3/7 substrate containing aminoluciferin. In the presence of caspase 3/7 this substrate is cleaved, aminoluciferin is released and consumed by luciferase (provided in the reaction mixture), generating a luminescent signal. The luminescent signal is proportional to the caspase activity present in the cells. The assay was carried out in A2780 and PC3 cells, plated in 96 wells, and incubated with the complex for 24 h, at a concentration equivalent to the IC_{50} found for each cell line. After 24 h, 100 μL of medium was removed from each well. Caspase 3/7® reagent was added in a 1:1 ratio and the plate was shaken in an orbital shaker for 30 s at 300–500 rpm. The plate was incubated at room temperature, protected from light for 1.5 h. The luminescence intensity was measured using an Infinite 200 Plate Reader (Tecan). Each experiment was repeated twice and each concentration was tested with at least three replicates. Results (mean \pm SD) were expressed as relative fluorescence units.

2.3.4.2. Hoechst staining assay. Hoechst dyes are cell permeable fluorophores used to stain DNA in living and fixed cells. These dyes are excited by UV light at around 350 nm, and emit blue-fluorescent light around a maximum at 461 nm. The assay was performed to look for signs of apoptotic markers in the PC3 cultures, such as DNA condensation, chromatin fragmentation, or formation of apoptotic bodies by using a fluorescence microscope. For the assay, PC3 cells at a concentration of 2.0×10^5 cells/mL were seeded on a coverslip

placed in a 6-wells plate and left to attach overnight. Then, cells were incubated in culture medium containing a concentration equivalent to the IC_{50} previously calculated of La-Nd-DPY or an equivalent concentration of the corresponding vehicle (DMSO, as a control) for 24 h or 48 h. After being washed with PBS, cells were fixed in 4% PFA for 15 min at room temperature, followed by three additional washing steps. Cells were then stained with a 1 $\mu\text{g/mL}$ solution of Hoechst for 20 min at room temperature (Hoechst 33342, Thermo Fisher Scientific), washed, and mounted in anti-fade mounting media (SlowFade™ Diamond Antifade Mountant, Invitrogen). The slides were imaged in a confocal microscope (Zeiss LSM 710) using a standard DAPI filter and $20\times$ magnification. At least 450 nuclei were analyzed in total from several random microscopic fields imaged per sample, in two independent experiments performed.

3. Results and discussion

3.1. Synthesis and characterization of the mixed complex La-Nd-DPY

The synthesis of the new mixed lanthanide(III) complex La-Nd-DPY was based upon the reaction of the diquatery salt-type pro-ligand *N,N'*-diphenacyl-4,4'-dipyridinium dibromide (DPB) with a mixture of lanthanum(III) sulfate and neodymium(III) sulfate in 2:1 M ratio, in methanol under reflux, in the presence of triethylamine (Et_3N). The latter reagent was used as a base which promoted the *in situ* transformation of the DPB pro-ligand into the dipyrindinium ylide-based ligand (Scheme 2), as was already shown by us in a recent work [27]. The new mixed Ln(III) complex was isolated in the form of a violet powder, which is air and moisture stable, and shows good solubility in dimethylsulfoxide and dimethylformamide, while it is poorly soluble in other common solvents like alcohols, acetone, acetonitrile and water. The violet color displayed by La-Nd-DPY indicated the transformation of DPB pro-ligand into its reactive intermediate DPY, induced by the basic trimethylamine [40]. Therefore, the resulting intermediate DPY is the ligand towards the complexation of both La(III) and Nd(III) ions.

Attempts to obtain single crystals for the mixed La-Nd-DPY complex, suitable for the X-ray structure determination, were so far unsuccessful, and therefore, the crystal structure is yet to be revealed. On the other hand, X-ray powder diffraction analysis revealed the amorphous nature of the complex. The experimental PXRD patterns for both the complex and the starting compounds, recorded for comparison, are given in Fig. 1. Nevertheless, different characterization tools, such as Fourier transform infrared spectroscopy (FTIR), elemental analysis (EA), electrospray ionization mass spectrometry (ESI-MS) ultraviolet–visible spectroscopy (UV–vis) and thermogravimetric analysis (TGA), were employed in order to propose the structure for La-Nd-DPY. The elemental analysis allowed to hypothesize its stoichiometric formula, being of the type $[\text{LaNd}(\mu_2\text{-DPY})(\mu_4\text{-SO}_4)_2(\text{Et}_3\text{N})]\text{Br}_2 \cdot 2\text{H}_2\text{OMeOH}$.

The infrared spectrum of the La-Nd-DPY mixed complex (Fig. 2) shows a number of weak and medium absorption bands located in the region $1640\text{--}1440 \text{ cm}^{-1}$, which are ascribed to the stretching vibrations of the $\text{C}=\text{C}$ and $\text{C}=\text{N}$ double bonds from both phenyl and pyridine rings present in the DPY ligand [41]. The strong and sharp absorption band at 1694 cm^{-1} , specific to the carbonyl ($\text{C}=\text{O}$) group from the DPB pro-ligand (Fig. 2), is no longer present in the IR spectrum of La-Nd-DPY, thus indicating the transformation of DPB pro-ligand into its dipyrindinium ylide intermediate DPY.

The broad band present in the range $3600\text{--}3200 \text{ cm}^{-1}$, together with the weak band at 1685 cm^{-1} can be assigned to the stretching and bending vibrations of clathrated water, possibly coming either from methanol, used as solvent in the synthesis, or from air. The weak bands at 1017 and 1057 cm^{-1} , recognizable for the bending vibrations of methine $\text{C}=\text{CH}$ and $\text{C}-\text{O}$ groups, respectively, resulted from the transformation of DPB into DPY [41]. From the strong and broad band located in the range $1200\text{--}990 \text{ cm}^{-1}$, the peaks at 990 cm^{-1} and those at 1061 , 1119 and 1169 cm^{-1} are observed, which are attributed to the

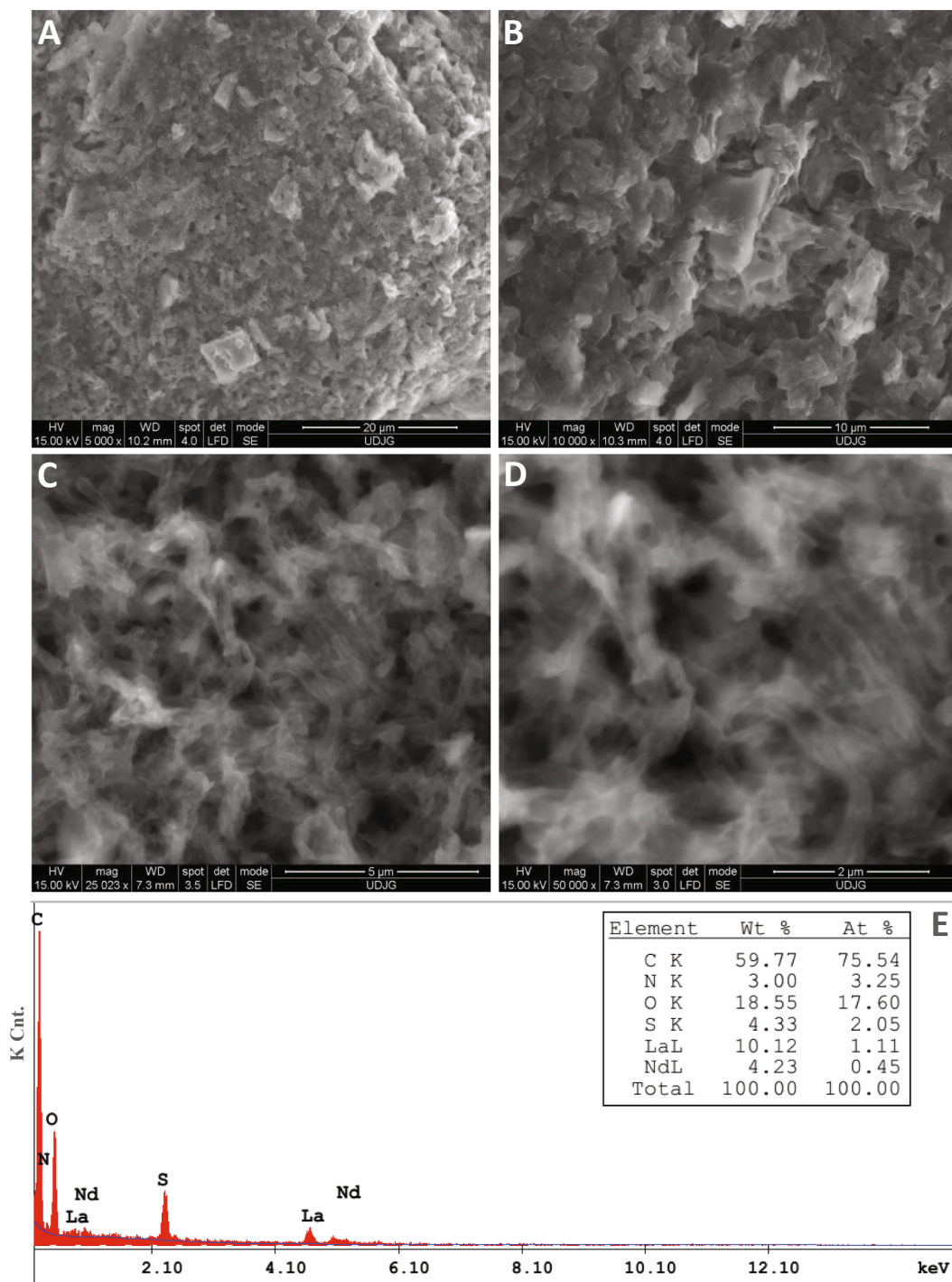


Fig. 8. A-D: SEM images of La-Nd-DPY at different magnifications; E: EDX spectrum acquired on a selected point from the 50.000x magnification image, along with the elemental composition.

ν_1 and ν_3 vibration modes, respectively, of the sulfate ions in the bridging bis-chelate mode [42]. Such a coordination mode of the sulfate ions was also encountered in, e.g., the samarium(III) complex (H₂prz) [Sm₂(HIDC)₂(SO₄)₂] (HIDC = imidazole-4,5-dicarboxylic monoacid, H₂prz = piperazine) [43], the mixed 3d-4f complex (H₂en)₂[La₂Co(SO₄)₆(H₂O)₂] (H₂en = diprotonated ethylenediamine) [44], and in our recently reported dinuclear homo-metallic Ln(III) complexes [Ln₂(μ₂-DPY)(μ₄-SO₄)(SO₄)₂(Et₃N)₂] (Ln = La or Nd) [27]. The medium band identified at 614 cm⁻¹ is assigned to the ν_4 bending [δ_d (OSO)] modes in the sulfate group [45]. In different papers reported in the literature for lanthanide complexes, the vibrations of Ln-N and Ln-O bonds were

attributed to, e.g., Nd-N = 437 cm⁻¹, Nd-O = 499 cm⁻¹ and La-N = 428 cm⁻¹, La-O = 492 cm⁻¹ [46], or La-N = 365 cm⁻¹, La-O = 435 cm⁻¹ and Nd-N = 366 cm⁻¹, Nd-O = 436 cm⁻¹ [47]. In the case of our new mixed complex, the medium absorption band observed at 410 cm⁻¹ was assigned to the Ln-N vibration, while the medium and broader band detected at 500 cm⁻¹ was assigned to the Ln-O vibration. This should be a clear indication that the Et₃N molecule is coordinated to the Ln(III) ions, instead of the water molecules, which are much less sterically hindering with respect to the former so to be able to enter the coordination sphere of the metal ions. Moreover, the presence of triethylamine in the mixed Ln(III) complex is evidenced by the weak

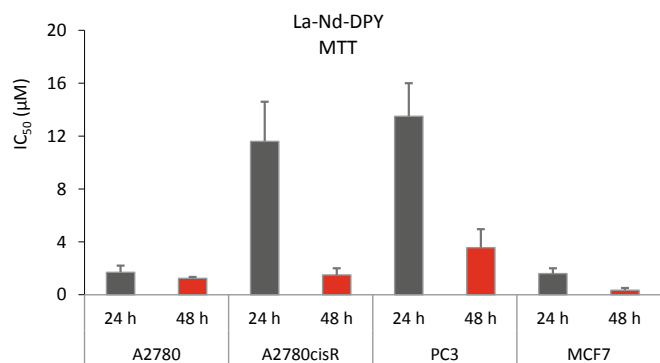


Fig. 9. Cytotoxic activity expressed as the IC_{50} values for **La-Nd-DPY** in the different types of cancer cells after 24 and 48 h incubation. Data are (mean \pm SD) of at least two independent experiments done with six replicates.

absorption band observed at 1216 cm^{-1} , which is assigned to the C–N vibration [42]. On the other hand, the occurrence of single bands related to the vibration of Ln–O and Ln–N bonds is indicative of the fact that the two Ln(III) ions have very close ionic radii, and thus, very similar vibrations, also considering the symmetric positions of the two enolic oxygen atoms from the DPY structure.

The UV–vis absorption spectra of **La-Nd-DPY** was recorded in DMSO and in the cell medium to ascertain the stability of the complex in both solutions. As can be observed from Fig. 3, the mixed complex is stable in DMSO at least for 1 h and very stable in the cellular medium (with 1% DMSO) at $37\text{ }^{\circ}\text{C}$ up to 72 h. The latter condition simulated the cellular medium at a maximum complex concentration ($100\text{ }\mu\text{M}$) and the experimental procedures with the cancer cells. The pro-ligand DPB by itself exhibits a single absorption band centered at 260 nm (Fig. 3, inset), attributed to intraligand (π – π^*) charge-transfer transitions [48]. The absorption band centered at 260 nm , was already encountered in our recently reported dinuclear homo-metallic Ln(III) complexes $[\text{Ln}_2(\mu_2\text{-DPY})(\mu_4\text{-SO}_4)(\text{SO}_4)_2(\text{Et}_3\text{N})_2]$ (Ln = La or Nd) (Fig. 3, inset) [27].

Thermogravimetric analysis (TGA) was used not only to assess the thermal stability of the mixed Ln(III) complex obtained, but also to evaluate the main weight losses recorded upon heating, and to confirm its hypothesized stoichiometric formulation. According to the TGA curve of **La-Nd-DPY** (Fig. 4), a first weight loss, amounting to ca. 14.15%, is registered in the temperature range $30\text{--}180\text{ }^{\circ}\text{C}$, which corresponds to the cumulative evolution of the two clathrated water molecules, one methanol molecule and one triethylamine molecule (theoretical loss: 14.12%). After this first event, the complex undergoes a progressive decomposition, whose decomposition onset was established at $200\text{ }^{\circ}\text{C}$, slightly lower than the decomposition onset recorded for the free DPB proligand, stable up to $225\text{ }^{\circ}\text{C}$, due to its quaternary ammonium nature [32]. The decomposition of the complex, continued until $500\text{ }^{\circ}\text{C}$, is accompanied by the weight loss of ca. 45.85%, which corresponds to the evolution of both DPY ligand and bromine (theoretical loss: 46.12%). The range from $500\text{ }^{\circ}\text{C}$ until the end of the heating process is left to the decomposition of the remaining inorganic Ln(III) sulfates.

The mass spectrum profile of the mixed complex (Fig. 5) suggests its fragmentations with the appearance of some intense characteristic peaks in the range $0\text{--}500$ (m/z), corresponding to the DPY ligand, and

Table 2

The comparison of the IC_{50} (μM) values found for **La-Nd-DPY** and cisplatin in the different types of cancer cells after 24 and 48 h incubation. Data are (mean \pm SD) of at least two independent experiments with six replicates each.

Compounds	A2780 24 h	A2780 48 h	A2780 cisR 24 h	A2780 cisR 48 h	PC3 24 h	PC3 48 h	MCF7 24 h	MCF7 48 h
La-Nd-DPY	1.7 ± 0.5	1.2 ± 0.1	12 ± 3.0	1.5 ± 0.5	14 ± 2.5	3.6 ± 1.4	1.6 ± 0.4	0.3 ± 0.2
Cisplatin	43 ± 10	14 ± 5.5	75 ± 15	44 ± 15	100 ± 10	57 ± 17	45 ± 18	20 ± 6.0

Table 3

The cytotoxic activity expressed as the IC_{50} (μM) of the lanthanide salts, the ligands, the mixed Ln complex and cisplatin in the A2780 ovarian cancer cell line up to 72 h. Data are (mean \pm SD) of at least two independent experiments with six replicates each.

Compounds	A2780 24 h	A2780 48 h	A2780 72 h
$\text{La}_2(\text{SO}_4)_3$	> 100	69 ± 11	72 ± 15
$\text{Nd}_2(\text{SO}_4)_3$	> 100	79 ± 15	71 ± 18
DPB	70 ± 15	30 ± 4.5	12 ± 2.6
DPY	32 ± 8.5	15 ± 4.2	19 ± 3.0
La-DPY	$40 \pm 9.0^*$	$6.3 \pm 1.5^*$	—
Nd-DPY	$30 \pm 11^*$	$3.6 \pm 1.5^*$	—
La-Nd-DPY	1.7 ± 1.1	1.2 ± 0.1	1.1 ± 0.2
Cisplatin	43 ± 10	14 ± 5.5	1.3 ± 0.1

* Data from Ref. [27].

very less intense peaks after m/z 500, corresponding to the lanthanide-based fragments (Table 1).

All the characterizations described above allowed the proposition of a structural model for the mixed complex **La-Nd-DPY** in the form of a coordination polymer, whose monomeric units are constituted by one DPY ligand, one La(III) ion, one Nd(III) ion, two sulfate groups and one triethylamine molecule. More in detail, one Ln(III) ion, either La(III) or Nd(III), is coordinated by one oxygen atom from the DPY ligand, four oxygen atoms from two bridging bis-chelate sulfate groups, and one nitrogen atom from triethylamine, therefore assuming six-coordination, and thus, an octahedral geometry. The other Ln(III) ion is coordinated by six oxygen atoms, of which two oxygen atoms coming from two distinct DPY ligands and four oxygen atoms coming from two bridging bis-chelate sulfate groups, are also assuming six-coordination, and thus, an octahedral geometry. Furthermore, a linear chain is formed by the sulfate groups bridging two alternate La(III) and Nd(III) ions, while the DPY and triethylamine ligands are disposed, also alternately coordinated to the Ln(III) ions, above and under the $-\text{La}(\text{SO}_4)\text{Nd}-$ chain to finally generate a linear coordination polymer (Fig. 6).

To the best of our knowledge, no other report has revealed such a type of linear chain built up with alternate Ln(III) ions bridged by the sulfate groups in a bis-chelate mode. On the other hand, the six-coordination of such Ln(III) ions, although still relatively rare, is joining the very scarce family of lanthanide-based complexes so far reported in the literature [27,49–52]. The higher coordination requirements of both La(III) and Nd(III) ions are likely causing the occurrence of a polymeric complex of **La-Nd-DPY**. However, the ‘large ionic radii – small coordination numbers’ relationship can be an interesting strategy attainable through the use of bulky ligands, such as DPY for the present case [50].

The redox behavior of **La-Nd-DPY** was evaluated by cyclic voltammetry (CV) experiments, both in methanol ($\text{pH} = 7.3$) and DMSO ($\text{pH} = 10.4$), which reveals that the oxidation/reduction potentials of the mixed complex are shifted towards positive or negative values attributed to its corresponding ligand (Fig. 7). OCP (open circuit potential) measurements on both solutions show slightly positive potentials, stable in time, with differences of ca. 20 mV to more positive values in methanol compared with DMSO, but it remains stable after 30 min in both solvents. An electrochemically reversible and partially chemically reversible one-electron reduction is observed in both solvents.

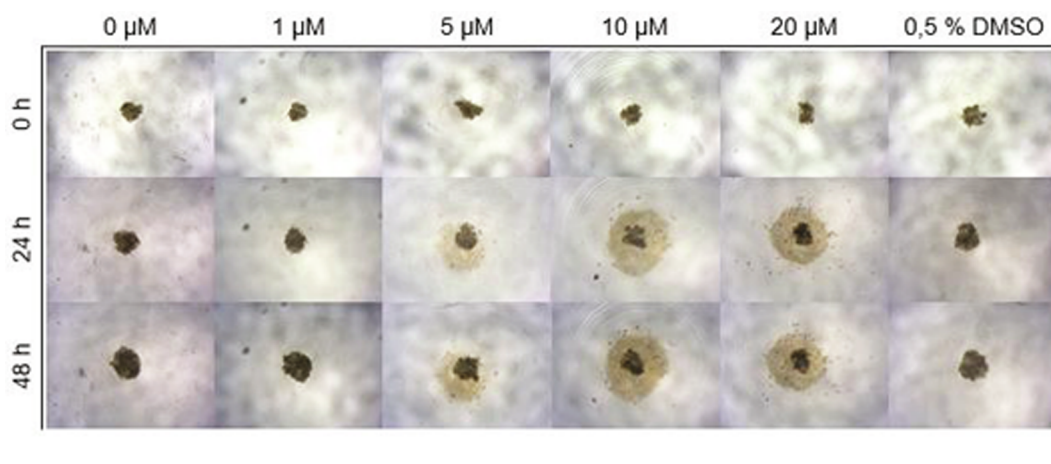


Fig. 10. Representative images of the PC3 spheroids before (0 h) and after (24 and 48 h) exposure to different concentrations of the mixed Ln complex. Controls consist of spheroids incubated only with medium (control) or with 0.5% DMSO (control vector).

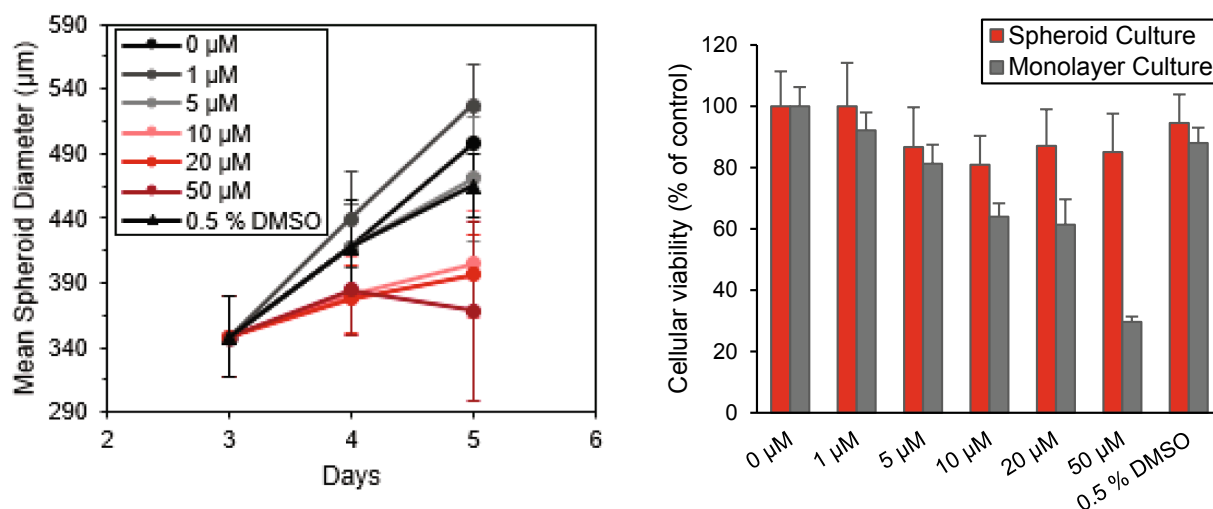


Fig. 11. Effect of exposure to the Ln complex on PC3 spheroids growth (left), represented by the mean spheroids diameter (in μm) as a function of the number of days in culture, and cellular viability at 48 h (right), assessed by the APH assay, in parallel to monolayer cultured cells. Controls consist of spheroids or monolayer cultured cells incubated only with medium or with 0.5% DMSO. Data are (mean \pm SD) of at least six replicates.

Cyclic voltammograms of the mixed complex in methanol revealed moderate electrochemical activity, starting at -0.5 V/E vs. $E_{\text{Ag}/\text{AgCl}/\text{sat}}$ ($E_{1/2} = 0.78$ V; for 100 mVs^{-1}) with an anodic current $I_{\text{pa}} = 6.55$ μA in DMSO and $I_{\text{pa}} = 13.2$ μA in methanol (double than in DMSO), as a result of more pairs of compound's ions obtained than free ions in this solvent, which are capable to exhibit reduction potential.

In both solvents the redox activity is observed, in negative and positive potential range. The registered current intensity depends on the working electrode (WE) used in the CV experiments. The intensity of the current is more relevant in DMSO (carbon-WE) at negative potential (from -0.56 V vs. $E_{\text{Ag}/\text{AgCl}/\text{sat}}$; $I_{\text{pa}} = 0.25$ μA), with a slightly constant increase for the next scan cycles (up to -0.53 V; $I_{\text{pa}} = 0.84$ μA) at 50 mVs^{-1} , and it has shown favorable change for the next electron transfer. In the same time, on Pt electrode (WE) the current intensity registered is less with 0.52 μA and at a potential of -0.58 V, after 10 consecutive cycles.

It is worth mentioning that the assessed redox potentials fall in the biologically relevant and accessible range. In proliferating cells, the reduction potential is about -0.24 V [53], while inside the tumor it is up to 100 mV lower. This means that the biological reducing agents, e.g., redox couple GSSG/2GSH, or ascorbic acid, are capable to reduce the synthesized compounds [54] and, according to our measurements, the biological reduction process of our mixed complex is possible.

Scanning electron microscopy (SEM) showed that the new mixed complex develops into quite uniform and homogeneous fibrillary net-like morphology with porous features, as can be observed at higher magnifications (Fig. 8, C and D). This kind of morphology is thus different from the homo-metallic La-DPY and Nd-DPY complexes, which exhibited multiform crystal structures and morphologies (elongated micro- and nanoparticles, aggregated micro- and nanoparticles) [27]. EDX analysis, acquired on a selected point from the highest magnification image, confirmed the presence of both lanthanide (III) ions in the mixed complex (Fig. 8, E).

3.2. Biological evaluation

3.2.1. Cytotoxic activity in cancer cell lines

The cytotoxic activity of La-Nd-DPY was evaluated in different cell lines representative of human cancers, such as ovarian A2780 and A2780cisR, sensitive and resistant to cisplatin respectively, prostate PC3 and breast MCF7 cells. Cisplatin was included in the assays for comparison, as it is the clinically approved metalloidrug used for cancer chemotherapy. The effect of the compounds on the cellular viability was evaluated by the MTT assay after incubation for 24 h and 48 h. As depicted in Fig. 9, La-Nd-DPY displayed consistently high cytotoxic activity for all cell lines upon 48 h of exposure to the compounds. At shorter

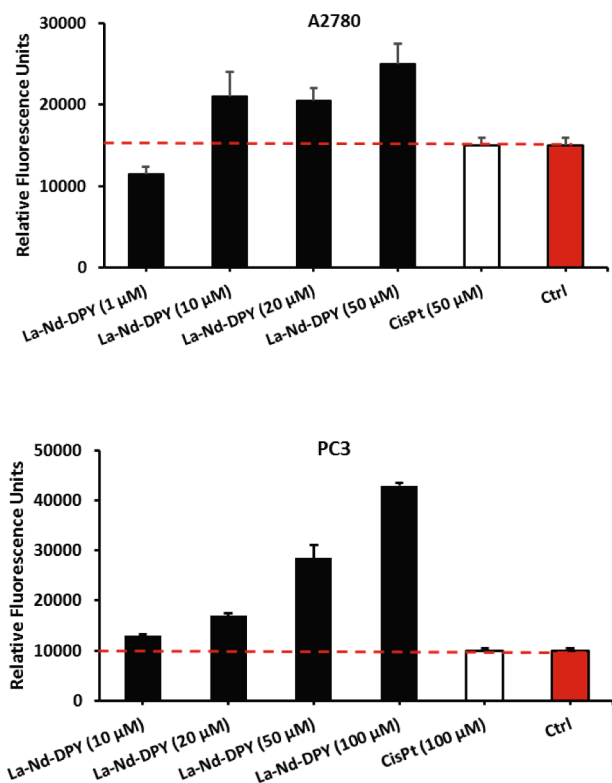


Fig. 12. ROS production by A2780 cells (top) and PC3 (down) upon 3 h exposure to La-Nd-DPY and cisplatin (cisPt) detected by the H₂DCFDA probe. Results in relative fluorescence units are representative of a typical experiment done with four replicates (mean \pm SD). Controls (Ctrl) consist of cells incubated only in medium.

incubation times (24 h), the cytotoxic profile differed in particular for the A2780cisR ovarian cells and the prostate cells. Cisplatin at both incubation times is less cytotoxic than the mixed Ln complex in all types of cells studied (Table 2), and, most importantly, in the cisplatin resistant cells and the PC3 cells known for their highly aggressive behavior [55].

The lanthanide sulfate salts were also included in this study and showed a very low cytotoxic effect, while the pro-ligand DPB showed a

moderate activity up to 48 h. At longer incubation times (72 h), DPB was more active but considerably less active than the corresponding Ln complex in the ovarian cells (Table 3). These results seem to confirm that neither the pro-ligand DPB nor the salt precursors seemed to be the active species responsible for the cytotoxicity observed. We also assessed the cytotoxicity of the DPY ligand, which was generated *in situ* from DPB, and observed that it presented some moderate cytotoxicity for prolonged incubation times.

The cytotoxic effect observed for the mixed Ln complex was far superior than cisplatin up to 48 h, and also higher than the one previously reported for the La-DPY (40 vs. 1.7 μ M) or Nd-DPY (30 vs. 1.7 μ M) complexes in the A2780 ovarian cells upon 24 h treatment or upon 24 h treatment in the MCF7 breast cells (La-DPY, 24 h: 43 vs. 1.6) [27].

3.2.2. Cytotoxic activity in cancer spheroids

Following the assessment of the cytotoxicity in human cancer cell lines, we evaluated the mixed complex in an advanced cancer cell model, multicellular tumor spheroids derived from the prostate cancer cell line PC3. This type of 3-dimensional culture method better recapitulates the *in vivo* microenvironment of tumors, in the sense that cells grow forming spheres that promote cell-cell and cell-ECM interactions, lacking in the conventional 2D culture. PC3 spheroids were allowed to grow for 3 days and then were incubated with La-Nd-DPY for 48 h. Images of PC3 spheroids that have been exposed to different concentrations of the mixed Ln complex are represented in Fig. 10.

As it is possible to discern in the photographic registries, spheroids size and shape were affected by the exposure to higher concentrations of the complex, as confirmed by the decrease in growth of PC3 spheroids upon exposure to the compound (Fig. 11, left). In particular, there was a decrease in the size of the spheroids incubated with the higher concentration (50 μ M), although there was already a noticeable delay in the growth of the spheroids, compared with the control, starting at 5 μ M. The viability results presented in Fig. 11 (right) show that, in comparison with the conventional monolayer cultures, in 3D spheroids the complex presents lower cytotoxicity (values of \sim 80% of the control at the higher concentrations). This is not surprising as 3D culture systems are frequently more refractory to anti-cancer treatments due to limited drug penetration and activation of several resistance mechanisms [56]. In fact, spheroid models can mimic the metabolic and proliferative gradients of *in vivo* tumors, with consequent changes in cellular phenotype and status, exhibiting multicellular chemoresistance.

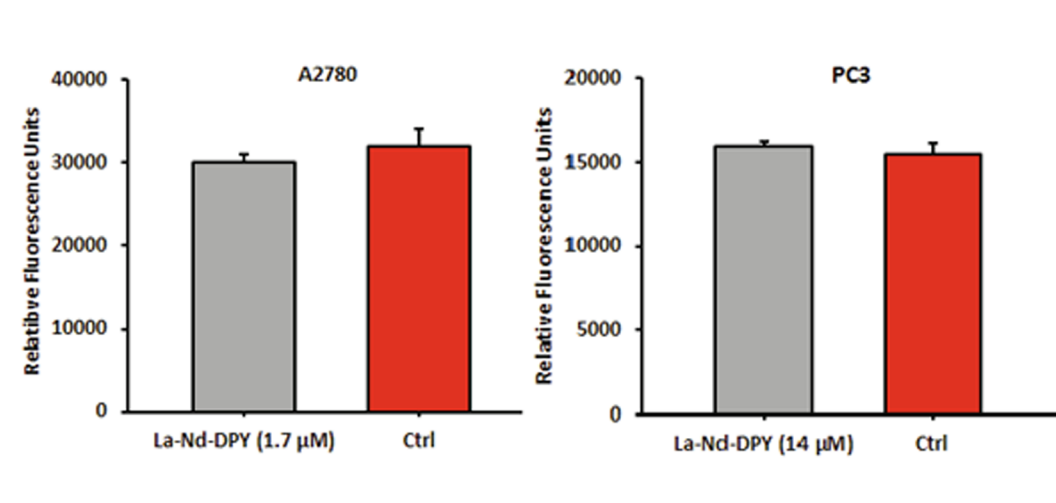


Fig. 13. Caspase -3 and -7 activity in A2780 cells (left) and PC3 cells (right), upon 24 h exposure to a concentration corresponding to the IC₅₀. Data was obtained from three replicates per condition and was expressed as the mean \pm SD from two independent assays, in relative fluorescence units.

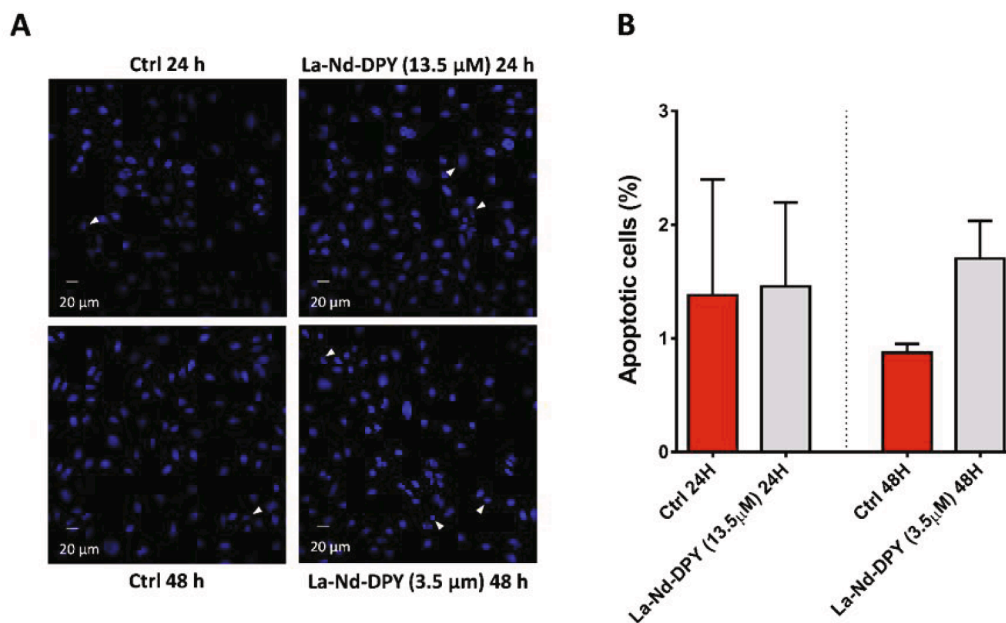


Fig. 14. Left: Representative images of PC3 cells stained with Hoechst 33,342 (A) in the absence (ctrl) or upon exposure to the complex (La-Nd-DPY) for 24 h (top) or 48 h (bottom). Right: Quantification (in %) of the number of apoptotic PC3 cells grown in the conditions described for A. The results are shown as mean values (\pm SD) obtained from two independent experiments in which at least 450 nuclei were counted per sample.

3.2.3. Production of ROS

The potential induction of intracellular ROS formation by La-Nd-DPY and cisplatin in A2780 and PC3 cells was analysed using the H₂DCFDA fluorescent probe, which can detect hydrogen peroxide, hydroxyl radicals or peroxyxynitrite. The effect of La-Nd-DPY and cisplatin on ROS production is presented in Fig. 12. The formation of ROS was evident for the mixed complex in a concentration-dependent mode for both cell lines. Concerning cisplatin, its cytotoxicity has been correlated to the generation of mitochondrial ROS that can promote a series of deleterious events and influence multiple metabolic functions, which may ultimately lead to cell death [57]. However, in the same experimental conditions, no detectable ROS seem to be produced by cisplatin, probably due to the short exposure time of 3 h required in the experimental method.

3.2.4. Apoptosis evaluation

3.2.4.1. Caspase activation. Apoptotic cell death is mediated by caspases, a family of cysteine proteases important for maintaining homeostasis through the regulation of cell death and inflammation [58]. To detect apoptotic events induced by the mixed Ln complex, the active form of caspases-3 and 7 were quantified in A2780 and PC3 cells [59]. As depicted in Fig. 13 the complex was unable to activate caspase-3/7 in these cell lines, since the values detected were similar to the ones obtained for control cells incubated only in media.

3.2.4.2. DNA fragmentation. In order to confirm the results obtained with the caspase activation assay, we performed a Hoechst nuclei staining assay to determine the percentage of apoptotic cells in a population of PC3 cells exposed, or not, to the La-Nd-DPY complex. The morphological hallmarks of apoptosis include DNA condensation, chromatin fragmentation, or formation of apoptotic bodies and, as such, we looked for signs of those apoptotic markers in our cultures. Corroborating the inability of this prostate cancer cell line to activate caspase-3/7 observed in the previous assay, we saw no statistically significant increase in the level of apoptosis on a cell population after exposure for 24 h or 48 h to IC₅₀ concentrations of the compound

(Fig. 14). This implies that the cell death observed on the cytotoxicity assay is not mainly due to apoptosis and that there are other pathways of cell death at play under these conditions.

4. Conclusions

The new mixed lanthanide(III) complex La-Nd-DPY was successfully prepared by the reaction of La(III) and Nd(III) sulfates with the diquaternary bis(pyridinium) salt DPB, acting as pro-ligand, in alcoholic ambient. The basic triethylamine, added in the reaction system, promoted the *in situ* conversion of DPB into the reactive ylide intermediate DPY, acting as ligand towards the complexation of both Ln(III) ions. All the characterization techniques described in this work allowed the disclosure of the possible structure for the new mixed Ln complex, thus featuring a 1-D polymeric chain, in which the Ln(III) ions are in the relatively rare six-coordination geometry. Cyclic voltammetry revealed the redox potentials of La-Nd-DPY, which were found to fall in the biologically relevant range. The cytotoxicity of the new mixed Ln complex is far superior than La-DPY or Nd-DPY, two complexes studied in a recent contribution, supporting the conclusion that the combined two Lns arrangement generate a new mixed Ln(III) complex with improved potential as an anticancer agent. Induction of apoptotic cell death does not seem to be the most relevant mechanism responsible for cellular cytotoxicity, as was the case of the previous La/Nd-DPY complexes. However, the cytotoxic mechanism seemed to be mediated by the generation of reactive oxygen species (ROS). Although speculative at present, the cytotoxicity of the new mixed Ln complex can be correlated to the generation of mitochondrial ROS that can influence multiple pathways that are known to sensitize cells towards suffering cell death. These findings will be worth of further investigation.

Declaration of Competing Interest

The authors declare that they have no known competing financial interests or personal relationships that could have appeared to influence the work reported in this paper.

Acknowledgements

This work was supported by an individual research grant of the Dunărea de Jos” University of Galați, contract number GI-01/2018 (A.T.) C²TN/IST authors gratefully acknowledge FCT support through the UID/Multi/04349/2013 project. The ESI-MS analyses were run on a QITMS instrument acquired with the support of RNEM – Portuguese Mass Spectrometry Network, ref. LISBOA-01-0145-FEDER-022125, financed by FCT and the Lisboa Regional Operational Programme (Lisboa2020), under the PT2020 Partnership Agreement, through the European Regional Development Fund (ERDF). The authors thank PhD Alina Cantaragiu from the “Dunărea de Jos” University of Galați for the helpful experimental assistance with the SEM-EDX analysis.

References

- [1] S.A. Cotton, Introduction to the Lanthanides, Lanthanide and Actinide Chemistry, John Wiley & Sons, West Sussex, 2006.
- [2] J.-C.G. Bünzli, Lanthanide coordination chemistry: from old concepts to coordination polymers, *J. Coord. Chem.* 67 (2014) 3706.
- [3] J.-C.G. Bünzli, C. Piguet, Taking advantage of luminescent lanthanide ions, *Chem. Soc. Rev.* 34 (2005) 1048.
- [4] K. Binnemans, Lanthanide-based luminescent hybrid materials, *Chem. Rev.* 109 (2009) 4283.
- [5] X. Liu, N. Wang, Q. Suo, Synthesis and luminescence properties of rare earth ternary complexes consisting of Tb(III), β -diketonates and 1,10-phenanthroline (phen), *Rare Metals* 27 (2008) 612.
- [6] K.L. Nash, D. Brigham, T.C. Shehee, A. Martina, The kinetics of lanthanide complexation by EDTA and DTPA in lactate media, *Dalton Trans.* 41 (2012) 14547.
- [7] R. Lyszczek, L. Mazur, Polynuclear complexes constructed by lanthanides and pyridine-3,5-dicarboxylate ligand: structures, thermal and luminescent properties, *Polyhedron* 41 (2012) 7.
- [8] M. Massi, M.I. Ogden, Luminescent lanthanoid calixarene complexes and materials, *Materials* 10 (2017) 1369.
- [9] Y. Hasegawa, Y. Kitagawa, Thermo-sensitive luminescence of lanthanide complexes, clusters, coordination polymers and metal-organic frameworks with organic photosensitizers, *J. Mater. Chem. C* 7 (2019) 7494.
- [10] M.S. Wickleder, Inorganic lanthanide compounds with complex anions, *Chem. Rev.* 102 (2002) 2011.
- [11] X.-H. Wu, N. Ren, J.-J. Zhang, Construction of three types of lanthanide complexes based on 3,4-dimethylbenzoic acid and 5,5'-dimethyl-2,2'-bipyridine: syntheses, structures, thermodynamic properties, luminescence, and bacteriostatic activities, *Appl. Organomet. Chem.* 32 (2018) e4528.
- [12] W.-H. Wang, H.-R. Tian, Z.-C. Zhou, Y.-L. Feng, J.-W. Cheng, Two unusual chiral lanthanide-sulfate frameworks with helical tubes and channels constructed from interweaving two double-helical chains, *Cryst. Growth Des.* 12 (2012) 2567.
- [13] A.D.G. Firmino, F. Figueira, J.P.C. Tomé, F.A. Almeida Paz, J. Rocha, Metal-Organic Frameworks assembled from tetraphosphonic ligands and lanthanides, *Coord. Chem. Rev.* 355 (2018) 133.
- [14] J.W. Cheng, G.Y. Yang, Hydrothermal synthesis of lanthanide and lanthanide-transition-metal cluster organic frameworks via synergistic coordination strategy, in: Z. Zheng (Ed.), *Recent Development in Clusters of Rare Earths and Actinides: Chemistry and Materials, Structure and Bonding*, Springer, Berlin, Germany, 2016.
- [15] Z. Zhang, Z. Zheng, Nanostructured and/or nanoscale lanthanide metal-organic frameworks, in: P. Cheng (Ed.), *Lanthanide Metal-Organic Frameworks. Structure and Bonding*, Springer, Berlin, Germany, 2014.
- [16] E.J. New, D. Parker, D.G. Smith, J.W. Walton, Development of responsive lanthanide probes for cellular applications, *Curr. Opin. Chem. Biol.* 14 (2010) 238.
- [17] R.D. Teo, J. Termini, H.B. Gray, Lanthanides: applications in cancer diagnosis and therapy, *J. Med. Chem.* 59 (2016) 6012.
- [18] S.P. Fricker, The therapeutic application of lanthanides, *Chem. Soc. Rev.* 35 (2006) 524.
- [19] G.-J. Chen, Z.G. Wang, X. Qiao, J.Y. Xu, J.L. Tian, S.P. Yan, Synthesis, DNA binding, photo-induced DNA cleavage and cell cytotoxicity studies of a family of light rare earth complexes, *J. Inorg. Biochem.* 109 (2012) 90.
- [20] Z.-M. Wang, H.-K. Lin, S.-R. Zhu, T.-F. Liu, Y.-T. Chen, Spectroscopy, cytotoxicity and DNA-binding of the lanthanum(III) complex of an l-valine derivative of 1,10-phenanthroline, *J. Inorg. Biochem.* 89 (2002) 97.
- [21] I. Kostova, G. Momekov, New cerium(III) complexes of coumarins – synthesis, characterization and cytotoxicity evaluation, *Eur. J. Med. Chem.* 43 (2008) 178.
- [22] G. Zhao, F. Li, H. Lin, H. Lin, Synthesis, characterization and biological activity of complexes of lanthanum(III) with 2-(1'-phenyl-2'-carboxyl-3'-aza-n-butyl)-1,10-phenanthroline and 2-(1'-p-phenol-2'-carboxyl-3'-aza-n-butyl)-1,10-phenanthroline, *Bioorgan. Med. Chem.* 15 (2007) 533.
- [23] M.P.C. Campello, E. Palma, I. Correia, P.M.R. Paulo, A. Matos, J. Rino, J. Coimbra, J.C. Pessoa, D. Gambino, A. Paulo, F. Marques, Lanthanide complexes with phenanthroline-based ligands: insights into cell death mechanisms obtained by microscopy techniques, *Dalton Trans.* 48 (2019) 4611.
- [24] W.-L. Kwong, R.W.-Y. Sun, C.-N. Lok, F.-M. Siu, S.-Y. Wong, K.-H. Low, C.-M. Che, An ytterbium(III) porphyrin induces endoplasmic reticulum stress and apoptosis in cancer cells: cytotoxicity and transcriptomics studies, *Chem. Sci.* 4 (2013) 747.
- [25] I. Kostova, R. Kostova, G. Momekov, N. Trendafilova, M. Karaivanova, Antineoplastic activity of new lanthanide (cerium, lanthanum and neodymium) complex compounds, *J. Trace Elem. Med. Biol.* 18 (2005) 219.
- [26] E. Brunet, O. Juanes, J.C. Rodriguez-Ubis, Supramolecularly organized lanthanide complexes for efficient metal excitation and luminescence as sensors in organic and biological applications, *Curr. Chem. Biol.* 1 (2007) 11.
- [27] A. Cârăc, R. Bosencu, R.M. Dinică, J.F. Guerreiro, F. Silva, F. Marques, M.P.C. Campello, C. Moise, O. Brîncoveanu, M. Enăchescu, G. Cârăc, A. Tăbăcaru, Synthesis, characterization and antitumor activity of two new dipyrindinium ylide based lanthanide (III) complexes, *Inorg. Chim. Acta* 480 (2018) 83.
- [28] J. Ding, C. Zheng, L. Wang, C. Lu, B. Zhang, Y. Chen, M. Li, G. Zhai, X. Zhuang, Viologen-inspired functional materials: Synthetic strategies and applications, *J. Mater. Chem. A* 7 (2019) 23337.
- [29] M. Baroncini, S. Silvi, A. Credi, Photo- and redox-driven artificial molecular motors, *Chem. Rev.* 120 (2020) 200.
- [30] M. Xu, S.P. Kelley, T.E. Glass, A multi-component sensor system for detection of amphiphilic compounds, *Angew. Chem. Int. Ed.* 130 (2018) 12923.
- [31] R. Papadakis, Mono- and di-quaternized 4,4'-bipyridine derivatives as key building blocks for medium- and environment-responsive compounds and materials, *Molecules* 25 (2020) 1.
- [32] B. Furdul, R.M. Dinica, A. Tabacaru, C. Pettinari, Synthesis and physico-chemical properties of a novel series of aromatic electron acceptors based on N-heterocycles, *Tetrahedron* 68 (2012) 6164.
- [33] A. Tabacaru, A.V. Dediu Botezatu, G. Horincar, B. Furdul, R.M. Dinica, Green accelerated synthesis, antimicrobial activity and seed germination test of quaternary ammonium salts of 1,2-bis(4-pyridyl)ethane, *Molecules* 24 (2019) 2424.
- [34] B. Furdul, G. Parfene, I. Ghinea, R. Dinica, G. Bahrim, M. Demeunynck, Synthesis and in vitro antimicrobial evaluation of new N-heterocyclic diquaternary pyridinium compounds, *Molecules* 19 (2014) 11572.
- [35] R. Dinica, B. Furdul, G. Bahrim, M. Demeunynck, New heterocycles precursors with biological interest, *Rev. Roum. Chim.* 53 (2008) 21.
- [36] J.K. Sun, X.D. Yang, G.Y. Yang, J. Zhang, Bipyridinium derivative-based coordination polymers: From synthesis to materials applications, *Coord. Chem. Rev.* 378 (2019) 533.
- [37] A. Tabacaru, R.M. Dinica, M. Cudalbeanu, C.M. Nicolescu, M. Bumbac, Catalytic effect of photoluminescent zinc oxide nanoparticles formed in the presence of quaternary ammonium salts, *Materials* 12 (2019) 2066.
- [38] R. Dinica, C. Pettinari, Synthesis of substituted 7,7'-bis-indolizines via 1,3-dipolar cycloaddition under microwave irradiation, *Heterocyclic Comm.* 7 (2001) 381.
- [39] M.V. Berridge, P.M. Herst, A.S. Tan, Tetrazolium dyes as tools in cell biology: new insights into their cellular reduction, *Biotechnol. Annu. Rev.* 11 (2005) 127.
- [40] I.I. Druta, R.M. Dinica, E. Bacu, I. Humelnicu, Synthesis of 7,7'-bisindolizines by the reaction of 4,4'-bipyridinium-ylides with activated alkynes, *Tetrahedron* 54 (1998) 10811.
- [41] R.M. Silverstein, F.X. Webster, D.J. Kiemle, D.L. Bryce, *Spectrometric Identification of Organic Compounds*, 8th Ed., John Wiley & Sons, Hoboken, New Jersey, 2014.
- [42] K. Nakamoto, *Infrared and Raman Spectra of Inorganic and Coordination Compounds*, Part B, 6th ed., John Wiley & Sons, Hoboken, New Jersey, 2009.
- [43] W.-G. Lu, D.-C. Zhong, L. Jiang, T.-B. Lu, Lanthanide coordination polymers constructed from imidazole-4,5-dicarboxylate and sulfate: syntheses, structural diversity, and photoluminescent properties, *Cryst. Growth Des.* 12 (2012) 3675.
- [44] Y.P. Yuan, R.-Y. Wang, D.-Y. Kong, J.-G. Mao, A. Clearfield, [H₂en]₂[La₂(SO₄)₆(H₂O)₂] (M = Co, Ni): first organically templated 3d-4f mixed metal sulfates, *J. Solid State Chem.* 178 (2005) 2030.
- [45] A. Sofetis, G.S. Papaefstathiou, A. Terzis, C.R. Raptopoulou, T.F. Zafropoulos, Preparation crystal structure and spectroscopic characterization of [Ga(OH)(SO₄)(terpy)(H₂O)]₂·H₂O (terpy = 2,2':6',2'-terpyridine): the first characterized gallium (iii) sulfato complex, *Z. Naturforsch.* 59b (2004) 291.
- [46] V.M. Naik, N.B. Mallur, Synthesis and characterization of lanthanide(III) Nitrate Complexes with terdentate ONO donor hydrazone derived from 2-benzimidazolyl mercaptoaceto hydrazide and o-hydroxy aromatic aldehyde, *J. Chem.* 8 (2011) 1900.
- [47] C.J. Athira, Y. Sindhu, M.S. Sujamol, K. Mohanan, Synthesis and spectroscopic characterization of some lanthanide(III) nitrate complexes of ethyl 2-[2-(1-acetyl-2-oxopropyl)azo]-4,5-dimethyl-3-thiophenecarboxylate, *J. Serb. Chem. Soc.* 76 (2011) 249.
- [48] H.H. Perkampus, *UV-Vis Spectroscopy and Its Applications*, Springer-Verlag, Berlin, 1992.
- [49] S. Liu, L.-W. Yang, S.J. Rettig, C. Orvig, Bulky ortho 3-methoxy groups on N₄O₃ amine phenol ligands producing six-coordinate bis(ligand)lanthanide complex cations [Ln(H₂O)₂]³⁺ (Ln = Pr, Gd; H₃L = tris((2-hydroxy-3-methoxybenzyl)amino)ethyl)amine), *Inorg. Chem.* 32 (1993) 2773.
- [50] K. Dahncke, A. Greiner, Unusual complex chemistry of rare-earth elements: large ionic radii – small coordination numbers, *Angew. Chem. Int. Ed.* 42 (2003) 1340.
- [51] S.A. Cotton, Establishing coordination numbers for the lanthanides in simple complexes, *Compt. Rend. Chim.* 8 (2005) 129.
- [52] B. Na, X.-J. Zhang, W. Shi, Y.-Q. Zhang, B.-W. Wang, C. Gao, S. Gao, P. Cheng, Six-coordinate lanthanide complexes: slow relaxation of magnetization in the dysprosium(III) complex, *Chem. Eur. J.* 20 (2014) 15975.
- [53] M. Ravera, S. Baracco, C. Cassino, P. Zanella, D. Osella, Appraisal of the redox behaviour of the antitumour ruthenium(III) complex [ImH][RuCl₄(DMSO)(Im)], *NAMI-A, Dalton Trans.* (2004) 2347.
- [54] M. Groessel, E. Reisner, C.G. Hartinger, R. Eichinger, O. Semanova, A.R. Timerbaev, M.A. Jakupcic, V.B. Arion, B.K. Keppler, Structure-activity relationships for NAMI-A-type complexes (HL)[trans-RuCl₄(S-dmsso)ruthenate(III)] (L = imidazole, indazole, 1,2,4-triazole, 4-amino-1,2,4-triazole, and 1-methyl-1,2,4-triazole):

- aquation, redox properties, protein binding, and antiproliferative activity, *J. Med. Chem.* 50 (2007) 2185.
- [55] S. Tai, Y. Sun, J.M. Squires, H. Zhang, W.K. Oh, C.-Z. Liang, J. Huang, PC3 is a cell line characteristic of prostatic small cell carcinoma, *Prostate* 71 (2011) 1668.
- [56] F. Mittler, P. Obeid, A.V. Rulina, V. Haguët, X. Gidrol, M.Y. Balakirev, High-content monitoring of drug effects in a 3D spheroid model, *Front. Oncol.* 7 (2017) 293.
- [57] R. Marullo, E. Werner, N. Degtyareva, B. Moore, G. Altavilla, S.S. Ramalingam, P.W. Doetsch, Cisplatin induces a mitochondrial-ROS response that contributes to cytotoxicity depending on mitochondrial redox status and bioenergetic functions, *Plos One* 8 (2013) e81162.
- [58] D.R. McIlwain, T. Berger, T.W. Mak, Caspase functions in cell death and disease, *Cold Spring Harb. Perspect. Biol.* 5 (2013) a008656.
- [59] M. Brentnall, L. Rodriguez-Menocal, R.L. De Guevara, E. Cepero, L.H. Boise, Caspase-9, caspase-3 and caspase-7 have distinct roles during intrinsic apoptosis, *BMC Cell Biol.* 14 (2013) 32.